Manassero, M. (1989). *Géotechnique* **39**, No. 2, 293–307

Stress–strain relationships from drained self-boring pressuremeter tests in sands

M. MANASSERO*

A simple numerical method to obtain the complete stress and strain paths during a drained self-boring pressuremeter test in sand is presented. Plane strain conditions and a material behaviour according to Rowe's (1962, 1972) dilatancy theory are assumed. The proposed method has been evaluated using a large number of self-boring pressuremeter tests on Ticino sand, performed in a calibration chamber. The comparison between the calculated values of peak shear resistance and the results obtained from conventional laboratory triaxial tests shows good agreement.

KEYWORDS: constitutive relations; field tests; sands; shear strength; strain; stress analysis

L'article présente une méthode numérique très simple pour obtenir les chemins complets des contraintes et des déformations au cours d'un essai pressiomètre autoforeur effectué dans du sable drainé. On admet des conditions de déformation plane et un comportement de la matière selon la théorie de dilatance de Rowe (1962, 1972). La méthode proposée a été évaluée en employant un grand nombre d'essais pressiomètre autoforeur effectués dans une chambre d'étalonnage sur du sable du Tessin. On trouve un bon accord entre les valeurs calculées de la réistance au cisaillement limite et les résultats obtenus à partir d'essais triaxiaux conventionnels effectués dans le laboratoire.

NOTATION

D	diameter of the pressuremeter
D_R	relative density
G	shear modulus
K_a^{cv}	ratio of minor principal stress to major principal stress when deformations is occurring at constant volume, $(\sigma_3/\sigma_1)_{cv}$
K_p^{cv}	principal stress ratio at constant volume, $(\sigma_1/\sigma_3)_{cv} = 1/K_a^{cv}$
L	length of the pressuremeter
p	radial stress at the cavity wall
p_0	initial horizontal stress
R, R_0	radius of the cavity and of the pressuremeter, initial value
R_{cc}	radius of the calibration chamber
r, r_0	radial distance, initial value
r	radial direction
s	isotropic stress in plane strain $(\sigma_1 + \sigma_3)/2$
s_C	isotropic stress in plane strain at point C
t	shear stress in plane strain $(\sigma_1 - \sigma_3)/2$
z	vertical direction
α	parameter describing the curved failure envelope (Baligh, 1976)
β	parameter for assessing the stress level at peak strength from proposed method
ρ_d/dzy	density
γ	shear strain
ε	tangential strain at the cavity wall $-\xi_R/R_0$
ε_v	volumetric strain
$\varepsilon_r, \varepsilon_\theta, \varepsilon_z$	radial, tangential and vertical strains
$\varepsilon_1, \varepsilon_2, \varepsilon_3$	principal strains
θ	tangential direction
ν	dilatancy angle at the peak strength $\sin^{-1}(-d\varepsilon_v/d\gamma)$
ξ	radial displacement
ξ_R	radial displacement at the cavity wall
σ	standard deviation
σ_0	reference stress equal to 1·0 kg/cm^2 = 98·2 kPa
σ_{ff}	normal stress on the failure surface at failure
$\sigma_r, \sigma_\theta, \sigma_z$	radial, tangential and vertical stresses
$\sigma_1, \sigma_2, \sigma_3$	principal stresses
τ_{ff}	shear stress on the failure surface at failure
ϕ	friction angle
ϕ_A	mobilized friction angle at point A
ϕ_{cv}	constant volume friction angle

Discussion on this Paper closes on 6 October 1989. For further details, see p. ii.

* Ingegneria Geotecnica, Torino, and Technical University of Torino.

ϕ_p peak friction angle
ϕ_p^{PS} peak friction angle in plane strain conditions from self-boring pressuremeter test
ϕ_p^{TX} peak friction angle in axial symmetric conditions from self-boring pressuremeter test
ϕ_p^{TXT} secant peak friction angle from laboratory triaxial test
ϕ_μ particle-to-particle friction angle
ϕ_0^{TXT} parameter describing the curved failure envelope (Baligh, 1976)

INTRODUCTION

The first closed-form solution for the problem of an expanding cavity was obtained considering a linear elastic material and small deformations (Lamé, 1852). Using this solution it is possible to determine only the elastic shear modulus G from the interpretation of both the first part of the self-boring pressuremeter test and the unload–reload cycles. Solutions for a linear elastic–perfectly plastic material were presented by Bishop *et al.* (1945) for a purely cohesive soil, and by Hill (1950), Ménard (1957), Chadwick (1959) and Vésic (1972) for a frictional and cohesive soil. On the basis of these general solutions Ladanyi (1972), Baguelin *et al.* (1972) and Palmer (1972) presented procedures for the interpretation of pressuremeter tests to obtain stress–strain relationships of any shape (i.e. strain softening and strain hardening) for cohesive soils, which deform with zero volume change (i.e. undrained conditions).

Considering granular material in the drained conditions, Ladanyi (1963), Vésic (1972), Wroth & Windle (1975), Hughes *et al.* (1977) and Robertson (1982) proposed procedures to determine the peak friction angle ϕ_p by assuming a linear elastic, perfectly plastic behaviour and taking into account the volume change developed when a shear stress is applied.

Ladanyi (1963) assumed that the volumetric strain stops when the maximum stress ratio has been reached, and introduced the total amount of volume change by trial and error. Vésic (1972) used the results of laboratory tests to input volume change. The method used by Wroth & Windle (1975) requires an assumption regarding the rate of volume change (dilatancy) at any instant during the cavity expansion and the method of Hughes *et al.* (1977) assumes that the rate of volume change is closely related to the friction angle developed at failure. This approach uses the concept of stress dilatancy proposed by Rowe (1962). However, to develop a simple closed-form solution Hughes *et al.* (1977) assumed that the rate of volume change was constant during the cavity expansion. This assumption has proved to be reasonable for very dense sands (Jewel *et al.* 1980) but less reliable for loose sands.

The method used by Robertson (1982) and Robertson & Hughes (1986) expands on the method of Hughes *et al.* (1977) by means of an empirical correction to account for the non-linear nature of the volume change during shear, especially for loose sands.

The method of interpretation of the self-boring pressuremeter test in sand presented in this Paper expands on the methods of Wroth & Windle (1975), Hughes *et al.* (1977) and Robertson (1982) by applying Rowe's stress dilatancy theory to model the complete non-linear nature of the stress and volume change behaviour during shear. The proposed method requires a numerical approach to solve the complete pressure–expansion data obtained from the self-boring pressuremeter test.

PROPOSED METHOD

The approach proposed is based on the following assumptions.

(*a*) Pressuremeter cavity expansion is plane strain, i.e. vertical strain, $\varepsilon_z = 0$.
(*b*) Elastic strains are neglected.
(*c*) Rowe's stress dilatancy theory is valid.

The assumption of plane strain cavity expansion is generally valid for pressuremeters with a large membrane length to diameter ratio L/D and for cavity expansion measured at the centre of the membrane up to about $\xi_R/R_0 = 10\%$, where $R_0 = D/2$.

Experimental results (Lade & Duncan, 1975; Lambrechts & Leonards, 1978; Ishihara, 1986) have shown that during deformation outside the yield locus elastic strains are negligible in relation to plastic strains. This is true in particular for sandy soils that are isotropically consolidated and sheared in simple shear.

Constitutive relationships

According to Rowe's (1962, 1972) theory, the behaviour of a stressed particular medium may be described by

$$\frac{\sigma_1 \, d\varepsilon_1}{\sigma_2 \, d\varepsilon_2 + \sigma_3 \, d\varepsilon_3} = -K_p^{cv} \qquad (1)$$

where

$$K_p^{cv} = (\sigma_1/\sigma_3)_{cv} = \frac{1 + \sin \phi_{cv}}{1 - \sin \phi_{cv}}$$

which is the constant volume principal stress ratio coefficient, where ϕ_{cv} is the constant volume friction angle.

Assuming plane strain conditions ($d\varepsilon_z = 0$), equation (1) reduces to

$$\frac{\sigma_1}{\sigma_3} = -K_p^{cv}\frac{d\varepsilon_3}{d\varepsilon_1} \tag{2}$$

Equation (2) can be considered valid for the complete stress–strain path of sands, and not only at the point where the maximum shear strength is mobilized (Rowe 1962, 1972). From this point of view equation (2) represents a flow rule for particulate material. Defining shear γ and volumetric ε_v strain as

$$\gamma = \varepsilon_1 - \varepsilon_3 \tag{3}$$

$$\varepsilon_v = \varepsilon_1 + \varepsilon_3 \tag{4}$$

and substituting ε_1 and ε_3 into equation (2) gives

$$\frac{\sigma_1}{\sigma^3} = K_p{}^{cv}\frac{1 - d\varepsilon_v/d\gamma}{1 + d\varepsilon_v/d\gamma} \tag{5}$$

As

$$(d\varepsilon_v/d\gamma)_{max} = -\sin\nu \tag{6}$$

equation (5) becomes the well-known formula

$$\left(\frac{\sigma_1}{\sigma_3}\right)_{max} = \frac{1+\sin\phi_p}{1-\sin\phi_p} = \frac{1+\sin\phi_{cv}}{1-\sin\phi_{cv}}\frac{1+\sin\nu}{1-\sin\nu} \tag{7}$$

where ν is the dilatancy angle at the peak shear strength, $(\sigma_1/\sigma_3)_{max}$ is the maximum stress ratio and ϕ_p is peak friction angle.

An example of an idealized trend of stress ratio σ_1/σ_3 plotted against shear strain γ for sandy soil is shown in Fig. 1(a). According to equations (2) and (5), Figs 1(b) and 1(c) show the complete strain paths for the idealized example.

In Fig. 1 material behaviour is divided into three main phases

(*a*) initial contractive behaviour, in which the material shows a decrease of volume and the mobilized shear strength is lower than the constant volume shear strength
(*b*) dilatant behaviour, in which the material shows an increase of volume and the mobilized shear strength is greater than the constant volume shear strength
(*c*) constant volume behaviour at large strains, in which the material shows no volume strains and the mobilized shear strength is equal to the constant volume shear strength.

Cavity expansion relationships

The equations of equilibrium and compatibility of strains around the cavity (Fig. 2) are

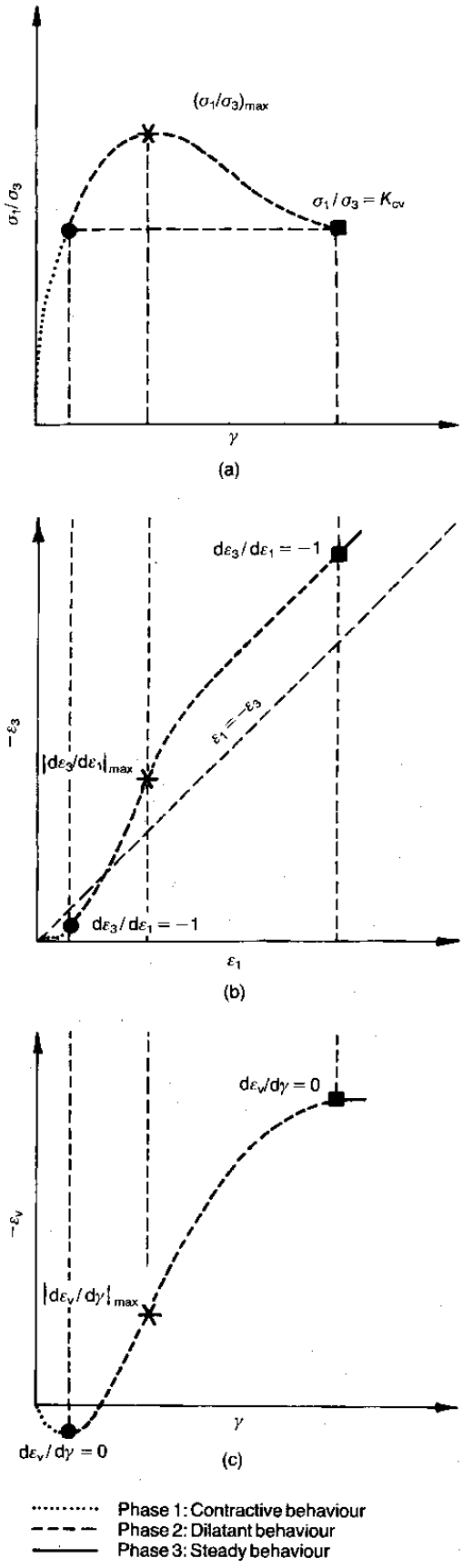

Fig. 1. Idealized stress–strain relationships in plane strain conditions from dilatancy theory

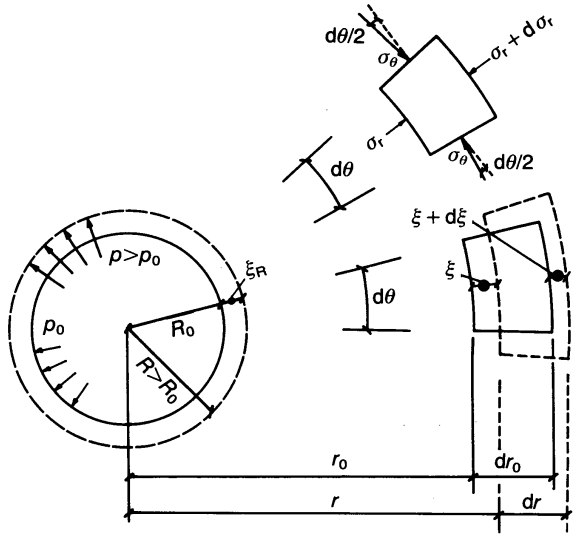

Compatibility equations

radial strain $\varepsilon_r = -\mathrm{d}\xi/\mathrm{d}r$

hoop strain $\varepsilon_\theta = -\xi/r$

At the cavity wall

cavity strain $\varepsilon = -\xi_R/R_0$

Equilibrium equation

$$\frac{\mathrm{d}\sigma_r}{\mathrm{d}r} = \frac{\sigma_\theta - \sigma_r}{r}$$

Fig. 2. Stresses and strains around the expanding cavity

$$\frac{\mathrm{d}\sigma_r}{\mathrm{d}r} = \frac{\sigma_\theta - \sigma_r}{r} \tag{8}$$

$$\frac{\mathrm{d}\varepsilon_\theta}{\mathrm{d}r} = \frac{\varepsilon_r - \varepsilon_\theta}{r} \tag{9}$$

where σ_r and σ_θ are the maximum and minimum principal stresses around the cavity (corresponding to σ_1 and σ_3), ε_r and ε_θ are the principal strains around the cavity (corresponding to ε_1 and ε_3) and r is the radial distance.

When combined with equation (2), equations (8) and (9) provide the solution of the expanding cylindrical cavity problem. Expressing them as a function of $r/\mathrm{d}r$ and referring them to a generic radius r around the expanding cavity, gives

$$\frac{\sigma_\theta - \sigma_r}{\mathrm{d}\sigma_r} = \frac{\varepsilon_r - \varepsilon_\theta}{\mathrm{d}\varepsilon_\theta} \tag{10}$$

Introducing

$$\sigma_\theta = -\frac{\sigma_r}{K_p^{cv}}\frac{\mathrm{d}\varepsilon_r}{\mathrm{d}\varepsilon_\theta}$$

into equation (10) from equation (2) and rearranging gives

$$\frac{\mathrm{d}\sigma_r}{\mathrm{d}\varepsilon_\theta} = -\frac{\sigma_r(1 + K_a^{cv}(\mathrm{d}\varepsilon_r/\mathrm{d}\varepsilon_\theta))}{\varepsilon_r - \varepsilon_\theta} \tag{11}$$

where $K_a^{cv} = 1/K_p^{cv}$.

Equation (11) is of general validity at any radius and can be solved for a soil element at the cavity wall where $\sigma_r = p$ and $\varepsilon_\theta = \varepsilon$ are measured during pressuremeter tests (see Fig. 2). To solve this equation analytically, involves the relationship $\varepsilon_r = \mathrm{f}(\varepsilon_\theta)$ (Hughes *et al.* 1977). However, as $p = \mathrm{F}(\varepsilon)$, equation (11) can be solved using numerical techniques.

Numerical analysis

The remaining unknown in the solution of equation (11) is ε_r. To evaluate ε_r at the cavity wall using a numerical procedure, the following equations can be established at the points i and $i-1$ on a pressure–expansion curve obtained from a self-boring pressuremeter test (Fig. 3)

$$\frac{\mathrm{d}p}{\mathrm{d}\varepsilon} = \frac{p(i) - p(i-1)}{\varepsilon(i) - \varepsilon(i-1)} \tag{12}$$

$$\frac{\mathrm{d}\varepsilon_r}{\mathrm{d}\varepsilon} = \frac{\varepsilon_r(i) - \varepsilon_r(i-1)}{\varepsilon(i) - \varepsilon(i-1)} \tag{13}$$

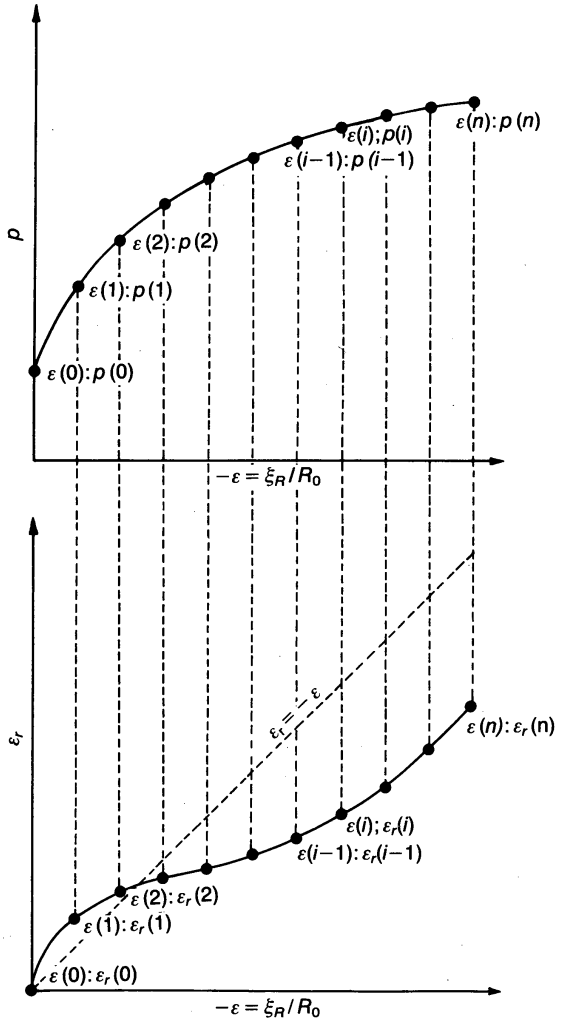

Fig. 3. Use of pressuremeter curve for numerical analysis

Substituting equations (12) and (13) into equation (11), using an average criterion between forward and backward interpolation results and rearranging gives

$$\varepsilon_r(i) = \frac{p(i)[\varepsilon(i-1) + K_a^{cv}\varepsilon_r(i-1)]}{2[p(i)(1 + K_a^{cv}) - p(i-1)]} - \frac{p(i-1)\varepsilon(i)}{2[p(i)(1 + K_a^{cv}) - p(i-1)]} + \frac{p(i)[\varepsilon(i-1) - \varepsilon_r(i-1)]}{2K_a^{cv}p(i-1)} + \frac{p(i-1)[\varepsilon_r(i-1)(1 + K_a^{cv}) - \varepsilon(i)]}{2K_a^{cv}p(i-1)} \quad (14)$$

Moreover, as $\varepsilon_r(0) = 0$, equation (14) allows the step by step computation of the unknown values of $\varepsilon_r(i)$ from $i = 1$ to $i = n$.

Once $\varepsilon_r(i)$, $\varepsilon(i)$, $p(i)$ and $\sigma_\theta(0) = p(0)$ are known, the deformation components $\gamma(i)$ and $\varepsilon_v(i)$ can be computed from equations (3) and (4). Then by solving equation (2) or equation (5), again using a finite difference technique, the complete stress–strain curve and stress path for the soil element at the cavity wall can be assessed.

The method proposed also allows the computation of stresses and strains at any radius r around the cavity. This is possible by solving numerically equations (8) and (9) once the complete stress–strain path of the basic soil element at the cavity wall is known.

VALIDATION OF PROPOSED METHOD

The method proposed has been evaluated using the results from pressuremeter tests performed in the ENEL-CRIS[1] calibration chamber (Bellotti *et al.* 1982). The tests were performed on dry, pluvially deposited Ticino sand and consist of two distinct stages. In the first stage the specimen is subject to one-dimensional straining to assign it the desired stress history. During this stage the constrained modulus of soil is measured. In the second stage, the pressuremeter expansion test is performed under strictly controlled conditions imposed at boundary stresses and/or strains. Constant vertical and horizontal stress boundary conditions were imposed for the pressuremeter tests considered in this Paper.

An ideal installation of the probe was simulated by placing the probe in the calibration chamber before pluvial deposition of the sand. The physical characteristics of Ticino sand are shown in Fig. 4. The following additional information was obtained in the laboratory.

[1] ENEL-CRIS: Italian national electricity board, hydraulic and structural research centre.

Sand		1 & 2 – Ticino
Dominant mineral		Quartz (30%)
Angularity (Lee's chart)		8 ÷ 9
Mica		~5%
ϱ_d max	1	1·705 t/m³
	2	1·700 t/m³
ϱ_d min	1	1·398 t/m³
	2	1·391 t/m³

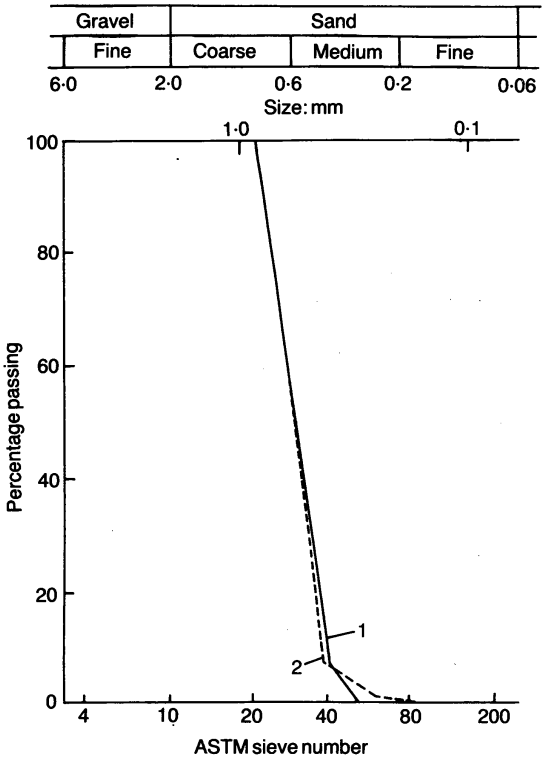

Fig. 4. Characteristics of the tested sand

The shear strength as obtained by performing triaxial tests on similarly pluvially deposited specimens of Ticino sand at various relative densities D_R, overconsolidation ratios (OCR) and confining stresses (Baldi *et al.* 1985). The results obtained show that failure envelopes referred to each D_R are not linear and can be approximated by means of the equation proposed by Baligh (1976)

$$\tan \phi_p^{TXT} = \tau_{ff}/\sigma_{ff} = \tan \phi_0^{TXT} + \tan \alpha \times \left(\frac{1}{2{\cdot}3} - \log_{10}\frac{\sigma_{ff}}{\sigma_0}\right) \quad (15)$$

where ϕ_p^{TXT} is the secant peak friction angle from triaxial tests, τ_{ff} is shear stress on the failure surface at failure, σ_{ff} is normal stress on the failure surface at failure, σ_0 is reference stress, assumed equal to 1·0 kg/cm² = 98·2 kPa, ϕ_0^{TXT} is the secant friction angle from triaxial tests at

$\sigma_{ff} = 2{\cdot}72\ \sigma_0$ and α is the angle which controls the curvature of the failure envelope. (When $\alpha = 0$ equation (15) reduces to the classical Mohr–Coulomb straight line relationship in the τ_{ff}–σ_{ff} plane. When α increases the curvature of the failure envelope increases.)

Equation (15) takes into account the influence of confining stresses and is described by soil parameters that can be easily and accurately determined from experimental results. The parameters ϕ_0^{TXT} and α, which describe the curved failure evelopes of three different classes of relative density, are summarized in Table 1. The simple linear interpolation or extrapolation has been adopted to evaluate these parameters and the corresponding ϕ_p^{TXT} values for others classes of D_R.

Values of ϕ_{cv} for Ticino sand were obtained using a ring shear appratus and ranged between 32° and 34°. Considering the stress level σ_{ff} during the analysed pressuremeter tests in the calibration chamber, a value of $\phi_{cv} = 34°$ was assumed (Fig. 5).

To check the reliability of Rowe's dilatancy theory (equation (1)), for Ticino sand, experimental results from triaxial tests were plotted using the appropriate parameters. Fig. 6 shows a typical example from a drained triaxial compression test on an isotropically consolidated sample of medium dense sand. In spite of a certain scatter in the experimental results, which is due mainly to the instability of the numerical derivation of $d\varepsilon_v/d\varepsilon_1$, on average the experimental data and the straight line with slope $K_p^{cv} = 3{\cdot}54$ agree well. This represents the theoretical behaviour of particulate material according to the Rowe's dilatancy theory, when $\phi_{cv} = 34°$.

Table 1. Summary of parameters defining shear strength envelope for Ticino sand

D_R: %	ϕ_0^{TXT}	α
45	38·2°	4·2°
65	40·2°	6·5°
85	42·9°	8·1°

The proposed algorithm was used by substituting the experimental readings from the pressuremeter test directly into equation (14). An example is given in Table 2.

An example of the stress–strain results is shown in Fig. 7, where isotropic stress in plane strain s is $(\sigma_r + \sigma_\theta)/2$ and shear stress in plane strain t is $(\sigma_r - \sigma_\theta)/2$.

In Fig. 7 scattering of the results is due to the numerical derivation procedure. A qualitative idea of the sand behaviour and an assessment of the peak friction angle in plane strain conditions ϕ_p^{PS} can be obtained from the maximum slope $(d\varepsilon_v/d\gamma)_{max}$ using

$$\left(\frac{\sigma_r}{\sigma_\theta}\right)_{max} = K_p^{cv}\,\frac{1 - (d\varepsilon_v/d\gamma)_{max}}{1 + (d\varepsilon_v/d\gamma)_{max}} = \tan^2\left(\frac{\phi_p^{PS}}{2} + \frac{\pi}{4}\right) \qquad (16)$$

To avoid numerical instability the pressuremeter data were fitted with a polynomial function (Fig. 8). It was observed that a polynomial degree of between 4 and 7 gives an acceptable fit for the needs of the method proposed and for the required precision in ϕ.

Examples of stress–strain relationships for test

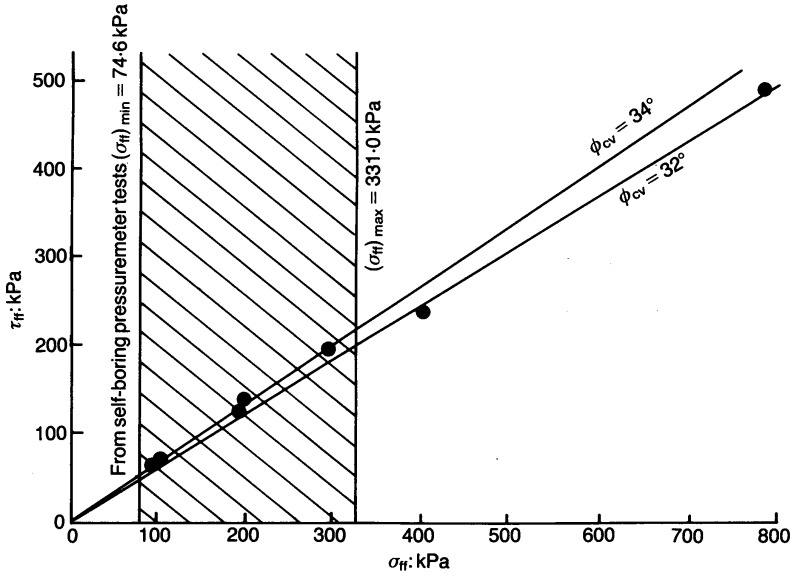

Fig. 5. Constant volume shear strength from ring shear apparatus

Table 2. Example of results of self-boring pressuremeter test 228

i	$-\varepsilon(i)$: %	$p(i)$: MPa	i	$-\varepsilon(i)$: %	$p(i)$: MPa	i	$-\varepsilon(i)$: %	$p(i)$: MPa
0	0·00000	0·2080	39	0·34645	0·4124	78	2·11714	0·8243
1	0·00350	0·2131	40	0·36219	0·4164	79	2·24836	0·8462
2	0·00700	0·2181	41	0·37794	0·4202	80	2·38134	0·8672
3	0·01225	0·2232	42	0·39194	0·4266	81	2·51781	0·8891
4	0·01575	0·2282	43	0·40594	0·4312	82	2·65953	0·9118
5	0·02100	0·2343	44	0·42168	0·4349	83	2·80826	0·9337
6	0·02625	0·2383	45	0·43393	0·4395	84	2·88174	0·9446
7	0·02974	0·2444	46	0·45143	0·4460	85	3·03221	0·9674
8	0·03849	0·2524	47	0·46893	0·4506	86	3·19143	0·0109
9	0·04199	0·2555	48	0·48117	0·4543	87	3·35065	1·1019
10	0·04724	0·2606	49	0·54591	0·4709	88	3·51336	1·0319
11	0·05424	0·2656	50	0·55991	0·4755	89	3·67958	1·0558
12	0·06124	0·2716	51	0·57216	0·4801	90	3·84929	1·0777
13	0·06649	0·2757	52	0·58966	0·4847	91	4·02950	1·0996
14	0·07174	0·2807	53	0·60190	0·4893	92	4·21146	1·1216
15	0·08049	0·2927	54	0·62115	0·4948	93	4·39517	1·1444
16	0·09099	0·2927	55	0·63690	0·4994	94	4·58588	1·1664
17	0·09789	0·2969	56	0·65440	0·5050	95	4·78184	1·1883
18	0·10673	0·3019	57	0·67189	0·5096	96	4·98129	1·2111
19	0·11548	0·3079	58	0·68939	0·5133	97	5·18425	1·2339
20	0·12598	0·3139	59	0·71039	0·5206	98	5·39595	1·2558
21	0·13473	0·3179	60	0·72613	0·5234	99	5·61289	1·2795
22	0·14348	0·3229	61	0·76463	0·5335	100	5·83684	1·3032
23	0·15398	0·3280	62	0·80312	0·5437	101	6·05904	1·3241
24	0·16622	0·3351	63	0·84511	0·5556	102	6·28823	1·3468
25	0·17672	0·3390	64	0·95884	0·5804	103	6·52617	1·3686
26	0·18722	0·3451	65	1·00084	0·5905	104	6·76586	1·3923
27	0·19597	0·3491	66	1·04108	0·6006	105	7·01430	1·4140
28	0·20997	0·3562	67	1·08132	0·6108	106	7·27498	1·4377
29	0·22047	0·3602	68	1·12507	0·6209	107	7·53216	1·4584
30	0·23096	0·3652	69	1·16881	0·6310	108	7·80334	1·4821
31	0·24321	0·3713	70	1·21255	0·6411	109	8·07802	1·5056
32	0·25546	0·3763	71	1·25804	0·6502	110	8·36144	1·5282
33	0·26596	0·3803	72	1·43301	0·6888	111	8·65186	1·5499
34	0·27996	0·3884	73	1·53099	0·7127	112	8·95103	1·5715
35	0·29395	0·3924	74	1·63773	0·7337	113	9·26594	1·5950
36	0·30795	0·3984	75	1·74971	0·7566	114	9·58785	1·6156
37	0·32020	0·4034	76	1·86693	0·7795	115	9·91325	1·6391
38	0·33420	0·4084	77	1·98766	0·8015	116	10·25265	1·6605

228 obtained using fifth, seventh and ninth order functions are shown in Fig. 9. The stress–strain and stress paths obtained with a polynomial fit procedure for tests 222 (loose to medium dense sand) and 228 (dense sand) are shown in Figs 10 and 11. In these figures point A is the end of pseudo-elastic behaviour recognized by a near-vertical part of the stress path in s–t plane. All the pressuremeter tests interpreted with the proposed method show an initial near-vertical part in the stress path before a sudden deviation. Point B is the end of contractive behaviour (phase 1) (i.e. maximum ε_v, $d\varepsilon_v/d\gamma = 0$ and $\sigma_r/\sigma_\theta = K_p^{cv}$) where constant volume shear strength is mobilized. Point C indicates the maximum dilatancy rate $(d\varepsilon_v/d\gamma)_{max}$ and stress ratio $(\sigma_r/\sigma_\theta)_{max}$ (i.e. fully mobilized peak friction angle). Point D is the end of dilatant and the start of constant volume behaviour (phase 3) (i.e. minimum ε_v, $d\varepsilon_v/d\gamma = 0$ and $\sigma_r/\sigma_\theta = K_p^{cv}$) where constant volume shear resistance is mobilized.

An example of the mobilized stress ratio and volumetric strain plotted against radius around the expanding pressuremeter cavity for test 228 is shown in Fig. 12. R_{cc} is the radius of the calibration chamber.

To obtain the peak friction angle ϕ_p and the maximum dilatancy angle v, 21 pressuremeter tests in the calibration chamber were interpreted using the proposed method and the procedures

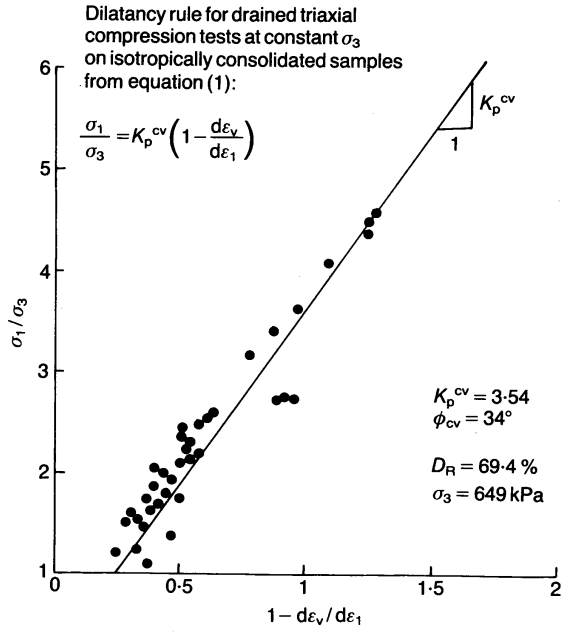

Fig. 6. Theoretical and experimental trends of laboratory triaxial test of Ticino sand according to dilatancy rule

suggested by Hughes *et al.* (1977) and Robertson (1982). The results are summarized in Table 3. They must be considered as peak friction angles under approximately plane strain conditions. To compare the plane strain peak friction angles from pressuremeter tests ϕ_p^{PS} with those obtained under axially symmetric conditions from triaxial tests ϕ_p^{TXT}, the following procedure was used (Fig. 13).

Considering the values of ϕ_p^{PS} from the interpretation methods of self-boring pressuremeter tests, the corresponding equivalent peak friction angle in axially symmetric conditions ϕ_p^{TX} was obtained on the basis of Lade & Lee's (1976) equation

$$\phi_p^{TX} = \frac{\phi_p^{PS} + 17°}{1{\cdot}5} \tag{17}$$

The laboratory triaxial values of ϕ_p^{TXT} at a given normal stress on the failure plane σ_{ff} were evaluated using the curved failure envelope equation

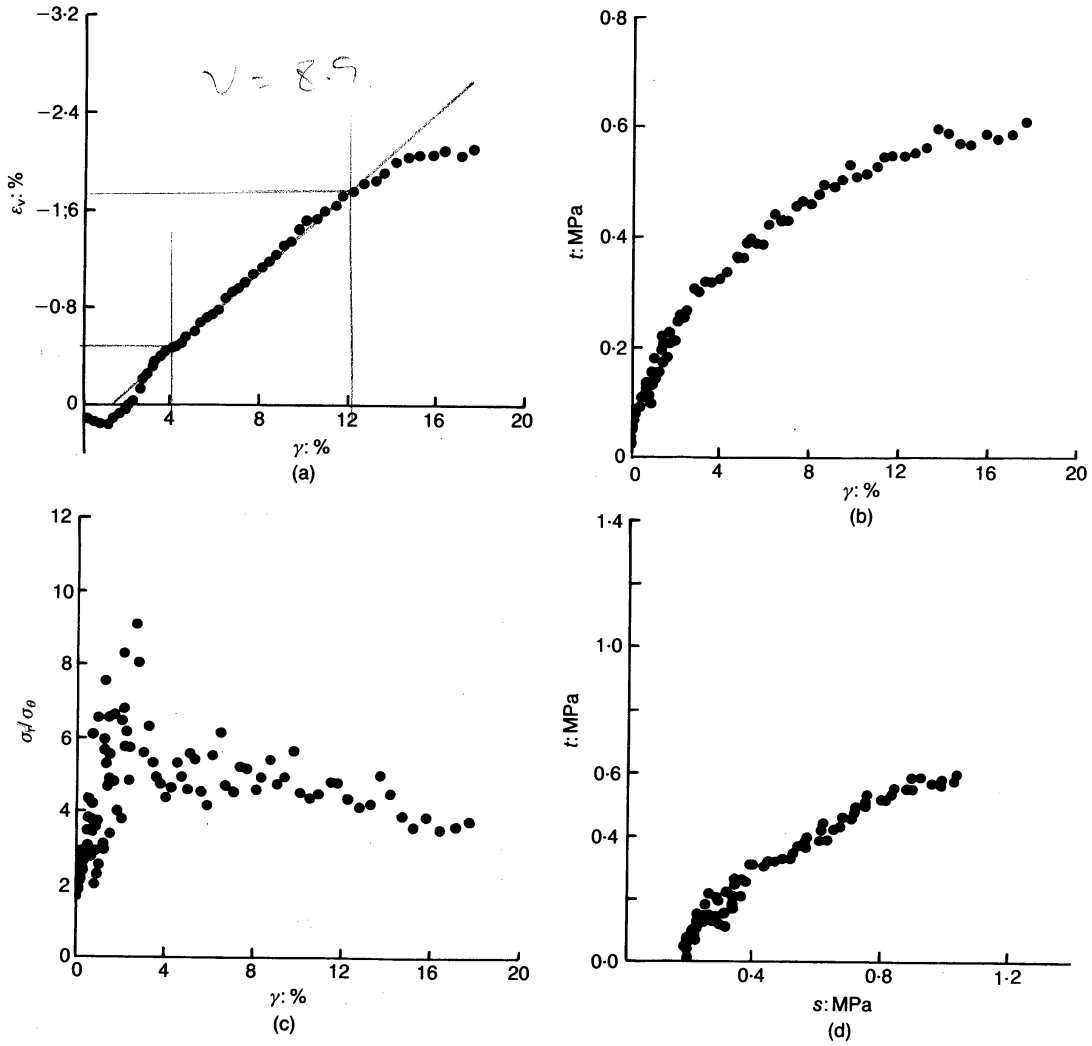

Fig. 7. Stress/strain relationships using the experimental readings from test 228 (D_R = 77·0%: (a) volumetric strain against shear strain; (b) shear stress against shear strain; (c) stress ratio against shear strain; (d) shear stress against mean normal stress

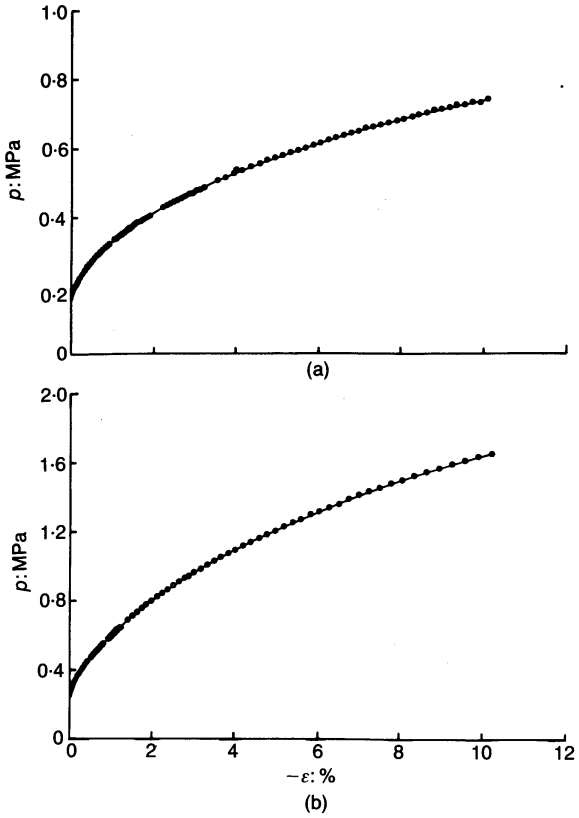

Fig. 8. Curve fitting results with seventh polynomial degree in original p against ε plot: (a) test 222; (b) test 228

and the parameters shown in Table 1. The value of σ_{ff} (Table 3) is calculated using the equation

$$\sigma_{ff} = s(1 - \sin^2 \phi_p^{TX}) \qquad (18)$$

where $s = p_0$, for elasto-plastic behaviour of soil around the cylindrical cavity (Hughes *et al.* 1977; Robertson, 1982), and $s = s_C$, where s_C is the isotropic stress under plane strain conditions at the peak stress ratio (point C in Fig. 11) for soil behaving according to dilatancy theory (proposed method).

To allow comparison between the results obtained in terms of ϕ_p^{TX} and ϕ_p^{TXT}, final values are plotted in Fig. 14.

Figure 14 shows that, on average, all the methods underestimate the peak friction angle given by the triaxial test ϕ_p^{TXT} at all the relative densities and confining stresses evaluated. The major disagreement arises using the method of Hughes *et al.* (1977). In the Author's opinion this method underestimates the peak friction angle mainly because of the simplified constitutive rule adopted. Robertson's (1982) method and the proposed method appear to offer a better agreement with the triaxial results, even if they determine slightly different values of σ_{ff} and subsequently ϕ_p^{TX} and ϕ_p^{TXT}.

From a close review of the results, it is possible

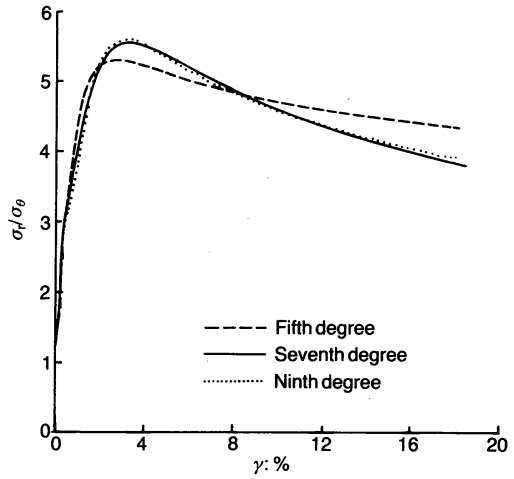

Fig. 9. Stress ratio–strain curve for fifth, seventh and ninth degree polynomials (test 228)

to observe that, in general, the main disagreement takes place for the overconsolidated specimens. Moreover, referring in particular to the results from the proposed method, normally consolidated specimens show, on average, good agreement with the laboratory triaxial peak friction angle.

This trend is shown clearly by the results given in Fig. 15, which plots, for two classes of density, the variation of ϕ according to Baligh's (1976) failure envelope from triaxial tests and results from interpretation of pressuremeter tests using the proposed method. For the normally consolidated specimens the decrease of peak friction angle, from the triaxial tests, with increasing normal stress on the failure plane, is in good agreement with the results obtained from the pressuremeter tests.

For the overconsolidated specimens, from interpretation of the pressuremeter tests, the peak friction angle seems to be influenced more by the overconsolidation ratio than by the normal stress on the failure plane. This is in conflict with experimental data reported by many authors (e.g. Baldi *et al.* 1985). In the Author's opinion these unreliable results are due mainly to the influence of boundary conditions in the vertical direction existing in the calibration chamber. When a normally consolidated specimen (with high vertical stress σ_z) is tested, it deforms under almost plane strain conditions, whereas when an overconsolidated specimen (with low vertical stress and constant stress boundary conditions) is tested, the vertical strains become important. Therefore, ε_z is not zero and the assumed plane strain conditions are no longer valid, and so the value of shear strength is lower.

Moreover, it is important to realize that referring to tests performed in calibration chamber the peak angle of friction derived using all the

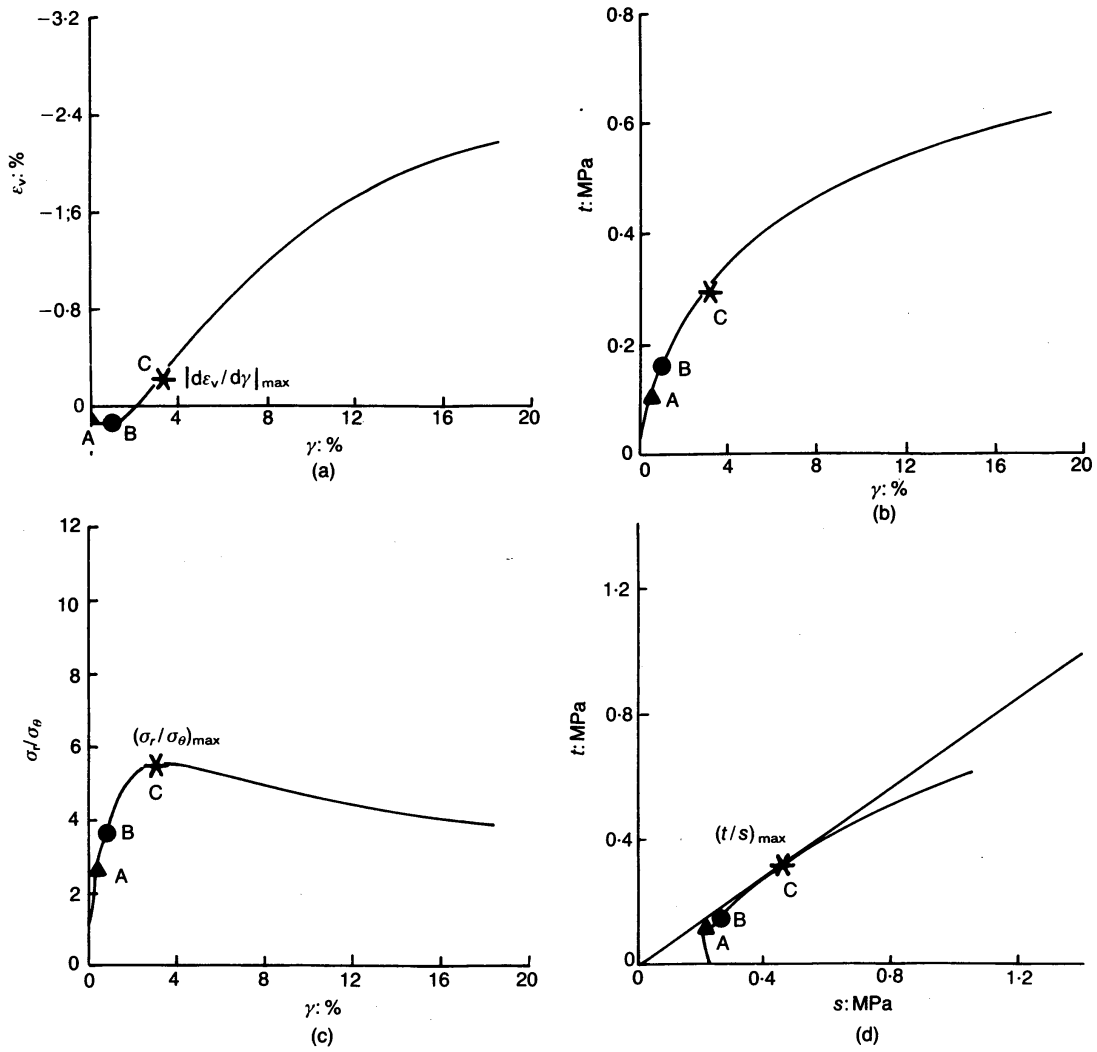

Fig. 10. Stress/strain relationships for test 228 (D_R = 77·0%): (a) volumetric strain against shear strain; (b) shear stress against shear strain; (c) stress ratio against shear strain; (d) shear stress against mean normal stress

methods previously mentioned, is influenced by the condition imposed at the radial boundary calibration chamber specimen (Fahey, 1980).

From a practical point of view, none of the pressuremeter curves analysed show any noticeable influence of radial boundary conditions, because of the large calibration chamber to pressuremeter diameter ratios ($2R_{cc}/2R_0 = 120/8{\cdot}2 \approx 14{\cdot}6$) and of the small radial displacement of the membrane at the end of the tests ($\xi_R \approx 4$ mm).

OTHER OBSERVATIONS

The points A, B, C, and D on the calculated stress–strain curves obtained using the proposed method, give important information both for the comprehension of sand behaviour and for the validation of the method.

From a plot of the mobilized friction angle at point A (ϕ_A) (end of pseudo-elastic behaviour) against peak friction angle it is possible to observe (Fig. 16) that ϕ_A values are in practice independent of peak friction angle and therefore of relative density D_R and confining stress. The average value of ϕ_A is about 24°. This value is very near the pure friction angle between quartz particles $\phi_\mu = 27°$ of Ticino sand.

This confirms that, before mobilizing the pure friction angle between particles surfaces, the sand behaviour is almost rigid (no slip between grains) and after, the sand strains increase rapidly, giving a typical non-linear–plastic stress–strain response.

Another important feature of sand behaviour around an expanding cavity, given by the proposed method, is the position of point C (peak shear strength) on the stress path plot (Fig. 17). The peak shear strength of sand is reached at a mean normal stress s_C much higher than that given by conventional interpretation methods of the self-boring pressuremeter test based on linear–elastic perfectly plastic material behaviour,

Table 3. Summary of calculated secant peak friction angles and dilatancy angles from pressuremeter tests

			Proposed method			Hughes *et al.* (1977)			Robertson (1982)		
Test	D_R: %	OCR	σ_{ff}: kPa	ϕ_p^{PS}: deg	ν: deg	σ_{ff}: kPa	ϕ_p^{PS} deg	ν: deg	σ_{ff}: kPa	ϕ_p^{PS}: deg	ν: deg
208	43·2	1·0	87·3	39·6	7·0	28·0	39·1	6·4	26·4	42·2	11·0
209	49·2	1·0	74·6	42·4	10·7	27·3	41·2	9·1	26·0	43·8	13·0
210	53·3	1·0	292·3	40·8	8·5	154·4	39·1	6·4	145·7	42·2	10·3
211	67·4	1·0	242·7	47·9	18·2	142·7	44·0	12·7	137·1	46·0	16·5
212	64·6	2·9	127·5	45·2	14·4	60·8	43·3	11·8	58·1	45·5	14·8
213	47·5	2·8	196·2	35·1	1·3	57·3	34·8	1·0	53·4	39·0	7·0
214	42·4	1·0	79·5	43·1	11·6	29·1	42·6	10·9	27·8	45·0	14·2
215	92·3	1·0	331·6	44·2	13·1	152·3	41·9	10·0	145·3	44·3	13·5
216	46·3	7·7	121·6	31·5	−3·0	52·6	31·1	−3·4	48·2	36·7	3·5
218	65·4	7·7	133·4	37·6	4·4	53·7	35·6	1·9	50·2	39·5	7·5
219	65·9	5·4	203·1	38·9	6·1	84·9	37·7	4·6	80·6	41·0	9·5
220	47·2	1·0	273·7	38·1	5·1	91·0	37·0	3·7	85·7	40·5	8·8
221	44·6	2·9	175·6	38·1	5·1	43·6	38·4	5·5	41·1	41·6	10·2
222	46·2	5·5	204·0	36·1	2·6	93·7	36·3	2·8	87·8	40·0	8·0
224	74·6	5·4	170·7	42·4	10·7	75·9	41·2	9·1	72·2	43·8	13·0
225	74·6	5·5	158·9	42·6	10·9	57·7	41·9	10·0	55·1	44·3	13·5
228	77·0	1·0	260·0	43·9	12·7	124·6	41·9	10·0	118·8	44·3	13·5
233	79·6	1·0	167·8	47·0	17·0	127·8	43·3	11·8	122·1	45·5	14·8
234	76·1	5·3	179·5	42·9	11·3	72·1	40·5	8·2	68·5	43·3	12·0
235	48·5	1·0	326·7	39·3	6·6	153·6	38·4	3·7	145·0	41·5	9·5
236	75·2	2·7	137·3	44·8	13·9	52·2	42·6	10·9	49·8	45·0	14·2

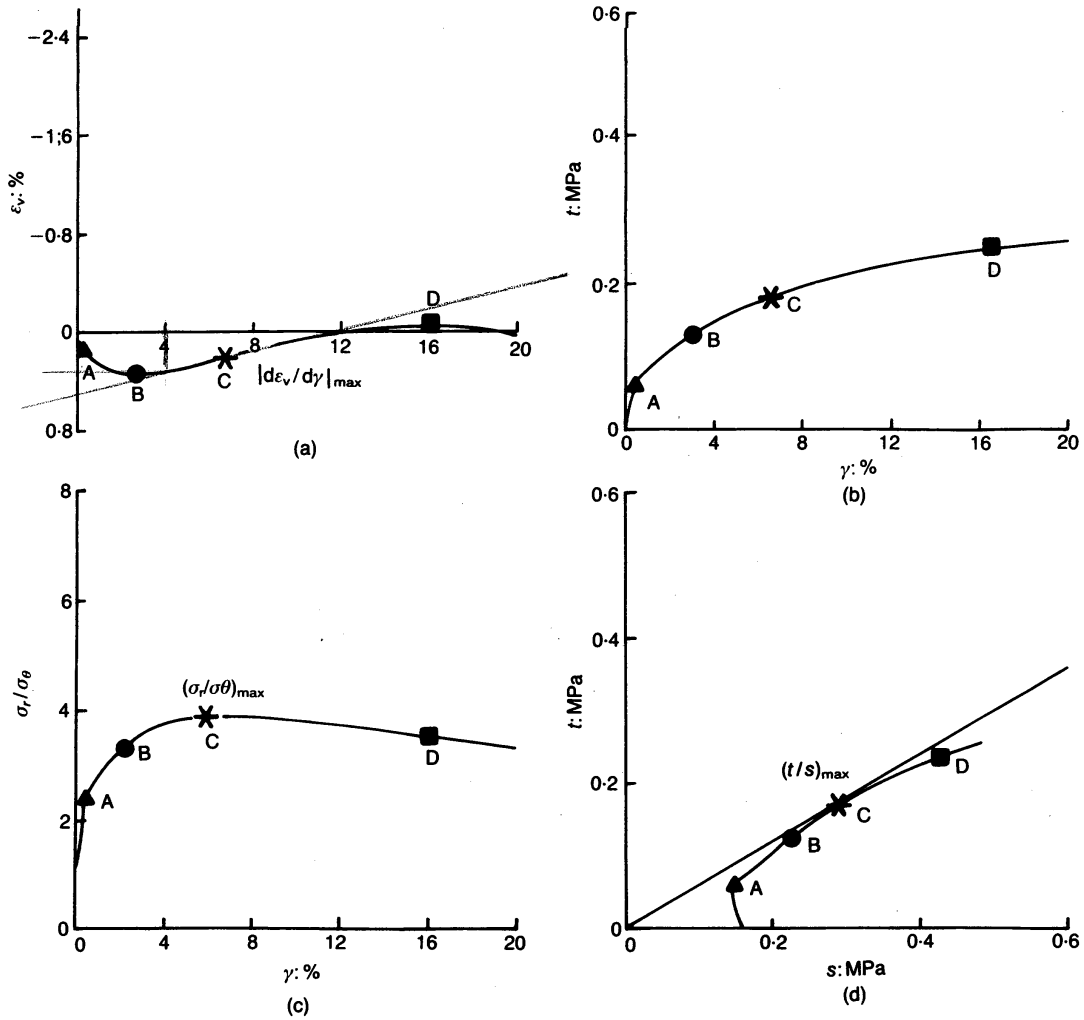

Fig. 11. Stress/strain relationships from test 222 (D_R = 46·2%): (a) volumetric strain against shear strain; (b) shear stress against shear strain; (c) stress ratio against shear strain; (d) shear stress against mean normal stress

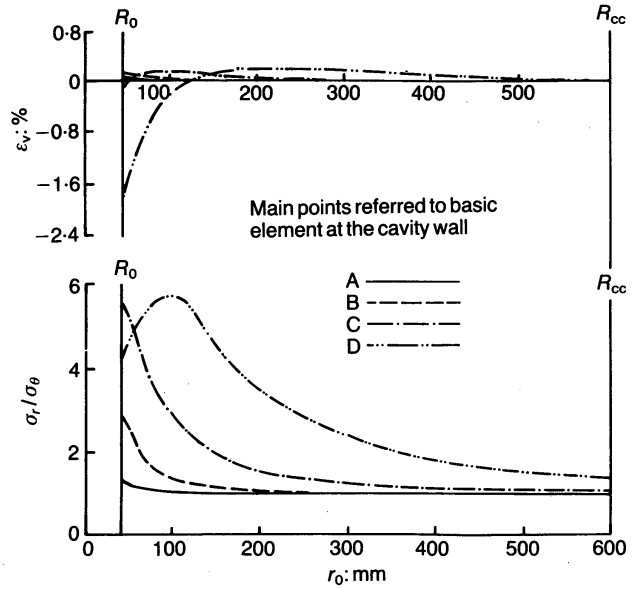

Fig. 12. Volumetric strain and stress ratio against radius around expanding cavity for test 228

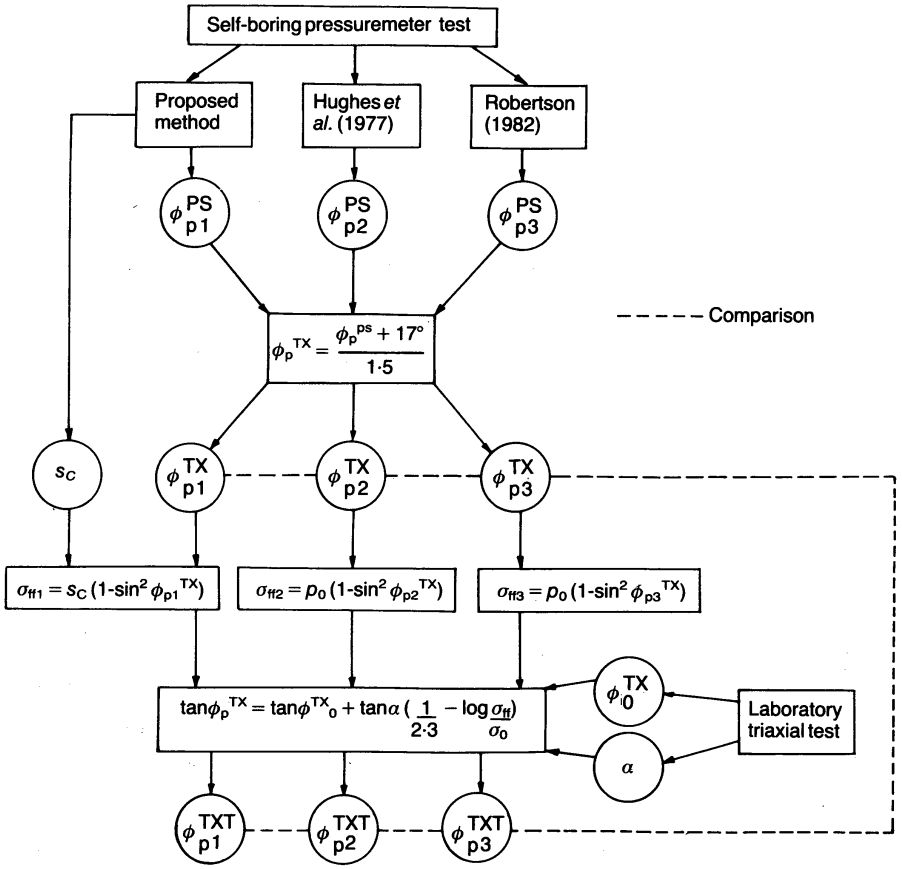

Fig. 13. Flow diagram of procedure to unify final results of secant peak friction angles from laboratory triaxial test and self-boring pressuremeter test interpretation methods

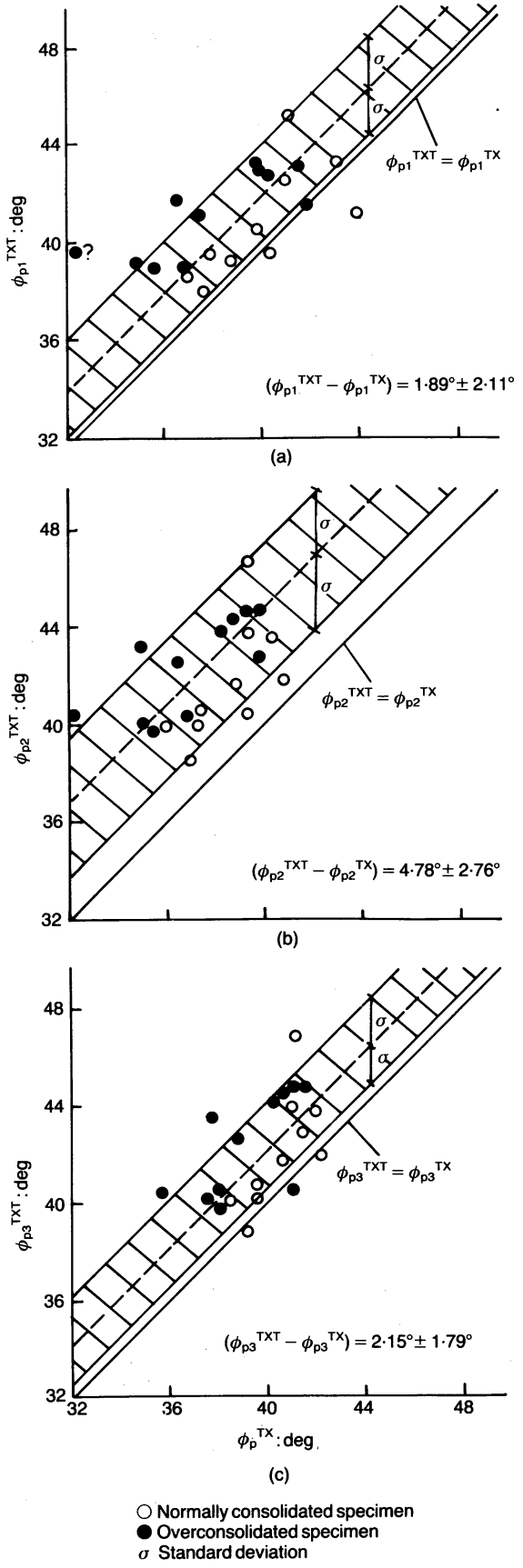

Fig. 14. Comparison between peak friction angles from self-boring pressuremeter test interpretation method and laboratory triaxial tests: (a) proposed methods: (b) Hughes *et al.* (1977) method; (c) Robertson (1982) method

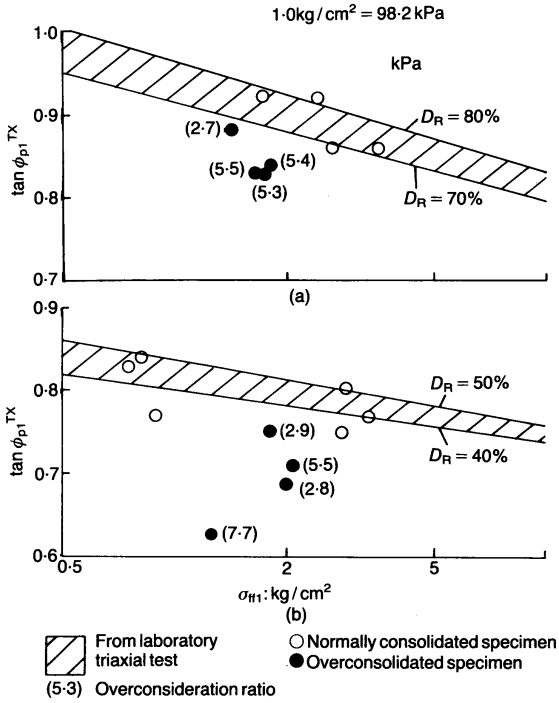

Fig. 15. Baligh's (1976) failure envelope from laboratory triaxial test and values from self-boring pressuremeter test interpretation with proposed method: (a) 70% < D_R < 80%; (b) 40% < D_R < 50%

where s at failure is still equal to the initial horizontal stress p_0.

Using an average value of β (Fig. 17) and accepting the hypothesis of the proposed method, it is possible to estimate the confining stress level which occurs at peak shear strength in the sand around an expanding pressuremeter knowing only p_0. Although not exact, this is more realistic than $s = p_0$.

CONCLUSION

A simple numerical solution has been presented for the expansion of a cylindrical cavity in sands. This procedure is based on the validity of Rowe's (1962, 1972) constitutive law, along the complete stress–strain curve and not only at the point of

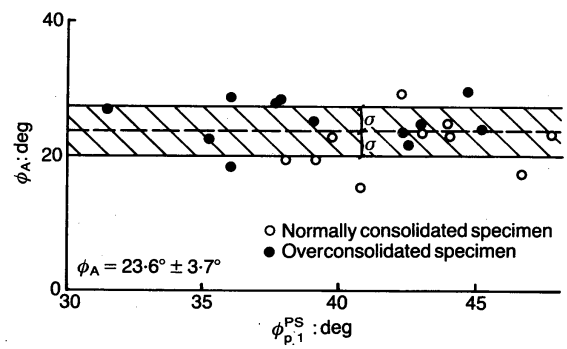

Fig. 16. Mobilized friction angle at the end of pseudo-elastic behaviour plotted against peak friction angle

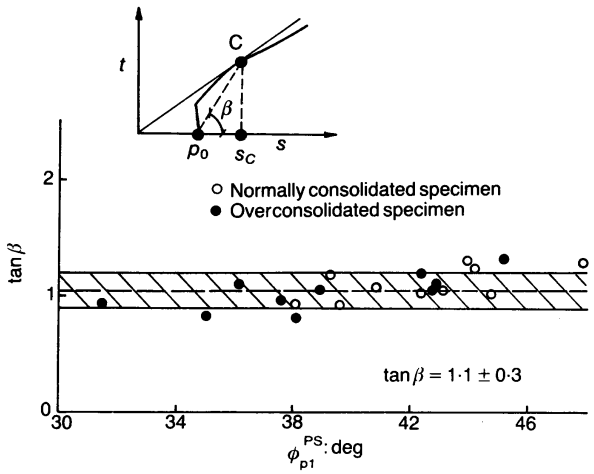

Fig. 17. Slope of $p_0 - c$ straight line against peak friction angle.

failure. By using this solution and adopting an appropriate numerical procedure it is possible to obtain the complete stress–strain relationships of the sand if the value of constant volume friction angle ϕ_{cv} is known.

The results, in particular those relating to peak shear strength, agree well with the well-established features of Ticino sand.

The application of the proposed solution to the 21 pressuremeter tests performed in the calibration chamber also looks promising in the determination of the complete stress–strain curve, the stress path, large strain shear strength and other features of sand behaviour.

It should be stressed that the proposed method was tested using pressuremeter tests performed under ideal conditions (the pressuremeter probe was inserted in the calibration chamber before specimen formation by pluvial deposition). It has therefore been proved only from a theoretical point of view.

From a practical point of view (i.e. to interpret true in situ self-boring pressuremeter tests) the proposed method needs further validation to assess the influence of initial disturbance that always occurs at the beginning of in situ tests using self-boring techniques and the influence of sand type, age, fines content and cementation in natural deposits.

ACKNOWLEDGEMENTS

The Author wishes to thank Dr P. Bertacchi and Dr R. Bellotti of ENEL-CRIS in Milan for making available the results of the pressuremeter tests performed in the calibration chamber, which were used to validate the method proposed in this Paper. Special thanks are due to Professor M. Jamiolkowski, Professor R. Lancellotta and Professor P. K. Robertson for stimulating discussions and important advice.

REFERENCES

Baguelin, F., Jézéquel, J. F., Lemèe, E. & Le Méhauté, A. (1972). Expansion of cylindrical probes in cohesive soils. *J. Soil Mech. Fdns Div. Am. Soc. Civ. Engrs* **98,** SM 11, 1129–1142.

Baldi, G., Bellotti, R., Crippa, V., Fretti, C., Ghionna, V., Jamiolkowski, M., Morabito, P., Ostricati, D. & Pasqualini, E. (1985). Laboratory validation of in situ tests. *Proc. 11th Int. Conf. Soil Mech., San Francisco,* 251–270.

Baligh, M. M. (1976). Cavity expansion in sand with curved envelopes. *J. Geotech. Engng Div. Am. Soc. Civ. Engrs* **102,** GT 11, 1131–1146.

Bellotti, R., Bruzzi, G. & Ghionna, V. (1982). Design, construction and use of a calibration chamber. *Proc. 2nd Eur. Symp. Penetration Test., Amsterdam* **2,** 439–446, Rotterdam: Balkema.

Bishop, R. F., Hill, R. & Mott, N. F. (1945). Theory of identation and hardness tests. *Proc. Phys. Soc.* **57,** 147.

Chadwick, P. (1959). The quasi-static expansion of a spherical cavity in metals and ideal soils. *Q. J. Mech. App. Math.* Part 1, **12,** 52–71.

Fahey, M. (1980). *A study of the pressuremeter test in dense sand.* PhD thesis, University of Cambridge.

Hill, R. (1950). *The mathematical theory of plasticity,* pp. 97–125. London: Oxford University Press.

Hughes, J. M. O., Wroth, C. P. & Windle, D. (1977). Pressuremeter tests in sands. *Géotechnique* **27,** No. 4, 453–477.

Ishihara, K. (1986). Evaluation of soil properties for use in earthquake response analysis. In *Geomechanical modelling in engineering practice,* pp. 241–275. Rotterdam: Balkema.

Jewell, R. J., Fahey, M. & Wroth, C. P. (1980). Laboratory studies of the pressuremeter test in sand. *Géotechnique* **30,** No. 4, 507–531.

Ladanyi, B. (1963). Evaluation of pressuremeter tests in granular soils. *Proc. 2nd Pan-Am. Conf. Soil Mech.* **1,** 3–30.

Ladanyi, B. (1972). In situ determination of undrained stress–strain behaviour of sensitive clays with the pressuremeter. *Can. Geotech. J.* **9,** No. 3, 313–319.

Lade, P. V. & Duncan, J. M. (1975). Elastoplastic stress–strain theory for cohesionless soil. *J. Geotech. Engng Div. Am. Soc. Civ. Engrs* **101,** GT 10, 1037–1053.

Lade, P. V. & Lee, K. L. (1976). *Engineering properties of soils,* pp. 145. Report UCLA-ENG-7652. University of California at Los Angeles.

Lambrechts, J. R. & Leonards, G. A. (1978). Effects of stress history on deformation of sand. *J. Geotech. Engng Div. Am. Soc. Civ. Engrs* **104,** GT 11, 1371–1387.

Lamé, G. (1852). *Leçons sur la théorie mathématique de l'élasticité des corps solides.* Paris: Bachelier.

Ménard, L. (1957). Mesure in situ des propriétés physiques des sols. *Annls Ponts Chauss.,* No. 14, 357–377.

Palmer, A. C. (1972). Undrained plane-strain expansion of a cylindrical cavity in clay: a simple interpretation of the pressuremeter test. *Géotechnique* **22,** No. 3, 451–457.

Robertson, P. K. (1982). In situ testing of soil with emphasis on its application to liquefaction assessment. PhD thesis, University of British Columbia.

Robertson, P. K. & Hughes, J. M. O. (1986). Determi-

nation of properties of sand from self-boring pressuremeter tests. In *The pressuremeter and its marine applications*. ASTM STP 950. Texas A & M: Philadelphia: American Society for Testing and Materials, 283–302.

Rowe, P. W. (1962). The stress-dilatancy relation for static equilibrium of an assembly of particles in contact. *Proc. R. Soc.*, Series A, **269**, 500–527.

Rowe, P. W. (1972). Stress–strain relationship for particulate materials at equilibrium. *Proceedings of the specialty conference on the performance of earth-supported structures, Purdue University*, pp. 327–359. New York: American Society of Civil Engineers.

Vésic, A. S. (1972). Expansion of cavities in infinite soil mass. *J. Soil Mech. Fdns Div. Am. Soc. Civ. Engrs* **98**, SM 3, 265–290.

Wroth, C. P. & Windle, D. (1975). Analysis of the pressuremeter test allowing for volume change. *Géotechnique* **25**, No. 3, 598–610.